



Elevation-dependent changes in *n*-alkane δD and soil GDGTs across the South Central Andes



Vanesa Nieto-Moreno^{a,*}, Alexander Rohrmann^b, Marcel T.J. van der Meer^c,
Jaap S. Sinninghe Damsté^{c,d}, Dirk Sachse^{e,b}, Stefanie Tofelde^{b,e}, Eva M. Niedermeyer^a,
Manfred R. Strecker^b, Andreas Mulch^{a,f}

^a Senckenberg Biodiversity and Climate Research Centre, Senckenberganlage 25, D-60325, Frankfurt am Main, Germany

^b Institut für Erd- und Umweltwissenschaften, Universität Potsdam, D-14476, Potsdam, Germany

^c NIOZ Royal Netherlands Institute for Sea Research, Department of Marine Microbiology and Biogeochemistry, and Utrecht University, P.O. Box 59, 1790 AB Den Burg, Texel, The Netherlands

^d Department of Earth Sciences, Faculty of Geosciences, Utrecht University, P.O. Box 80.121, 3508 TA Utrecht, The Netherlands

^e GFZ German Research Centre for Geosciences, Section 5.1: Geomorphology, Telegrafenberg, D-14473, Potsdam, Germany

^f Institut für Geowissenschaften, Goethe Universität Frankfurt, D-60438, Frankfurt am Main, Germany

ARTICLE INFO

Article history:

Received 18 April 2016

Received in revised form 29 June 2016

Accepted 27 July 2016

Available online 29 August 2016

Editor: A. Yin

Keywords:

South Central Andes
leaf-wax *n*-alkane δD
branched GDGTs
MAT_{mir} paleothermometer
paleoaltimetry proxies
altitudinal transects

ABSTRACT

Surface uplift of large plateaus may significantly influence regional climate and more specifically precipitation patterns and temperature, sometimes complicating paleoaltimetry interpretations. Thus, understanding the topographic evolution of tectonically active mountain belts benefits from continued development of reliable proxies to reduce uncertainties in paleoaltimetry reconstructions. Lipid biomarker-based proxies provide a novel approach to stable isotope paleoaltimetry and complement authigenic or pedogenic mineral proxy materials, in particular outside semi-arid climate zones where soil carbonates are not abundant but (soil) organic matter has a high preservation potential. Here we present δD values of soil-derived *n*-alkanes and mean annual air temperature (MAT) estimates based on branched glycerol dialkyl glycerol tetraether (brGDGT) distributions to assess their potential for paleoelevation reconstructions in the southern central Andes. We analyzed soil samples across two environmental and hydrological gradients that include a hillslope (26–28°S) and a valley (22–24°S) transect on the windward flanks of Central Andean Eastern Cordillera in NW Argentina. Our results show that present-day *n*-alkane δD values and brGDGT-based MAT estimates are both linearly related with elevation and in good agreement with present-day climate conditions. Soil *n*-alkanes show a δD lapse rate ($\Delta(\delta D)$) of $-1.64\text{‰}/100\text{ m}$ ($R^2 = 0.91$, $p < 0.01$) at the hillslope transect, within the range of δD lapse rates from precipitation and surface waters in other tropical regions in the Andes like the Eastern Cordillera in Colombia and Bolivia and the Equatorial and Peruvian Andes. BrGDGT-derived soil temperatures are similar to monitored winter temperatures in the region and show a lapse rate of $\Delta T = -0.51\text{ °C}/100\text{ m}$ ($R^2 = 0.91$, $p < 0.01$), comparable with lapse rates from *in situ* soil temperature measurements, satellite-derived land-surface temperatures at this transect, and weather stations from the Eastern Cordillera at similar latitude. As a result of an increasing leeward sampling position along the valley transect lapse rates are biased towards lower values and display higher scatter ($\Delta(\delta D) = -0.95\text{‰}/100\text{ m}$, $R^2 = 0.76$, $p < 0.01$ and $\Delta T = -0.19\text{ °C}/100\text{ m}$, $R^2 = 0.48$, $p < 0.05$). Despite this higher complexity, they are in line with lapse rates from stream-water samples and *in situ* soil temperature measurements along the same transect. Our results demonstrate that both soil *n*-alkane δD values and MAT reconstructions based on brGDGTs distributions from the hillslope transect ($\Delta(\delta D) = -1.64\text{‰}/100\text{ m}$, $R^2 = 0.91$, $p < 0.01$ and $\Delta T = -0.51\text{ °C}/100\text{ m}$, $R^2 = 0.91$, $p < 0.01$) track the direct effects of orography on precipitation and temperature and hence the combined effects of local and regional hydrology as well as elevation.

© 2016 Elsevier B.V. All rights reserved.

1. Introduction

Orogenic surface uplift and associated topographic evolution of tectonically active mountain belts collectively exert a strong im-

* Corresponding author. Fax: +49 69 7542 7906.

E-mail address: Vanesa.Nieto-Moreno@senckenberg.de (V. Nieto-Moreno).

impact on global atmospheric circulation patterns, long and short-term erosion rates, distribution of biomes, and precipitation patterns (e.g., Poulsen et al., 2010; Mulch, 2016). Understanding and quantifying the underlying drivers shaping the evolution of topography in ancient and active orogens permits to disentangle some of the dynamic interactions and feedbacks among surface uplift, climate, erosion and sedimentation over both short-term and geological time-scales (e.g., Rowley and Garzzone, 2007; Garzzone et al., 2008; Ehlers and Poulsen, 2009; Hoorn et al., 2013).

One increasingly popular tool to reconstruct paleoelevation in continental plateau regions is stable isotope paleoaltimetry (e.g., Chamberlain et al., 1999; Garzzone et al., 2000; Rowley et al., 2001; Rowley and Garzzone, 2007; Mulch et al., 2008; Gébelin et al., 2013). Stable isotope paleoaltimetry relies on systematic changes in the oxygen ($\delta^{18}\text{O}$) or hydrogen (δD) isotopic composition of precipitation that occur when moist air masses rise and cool during their ascent (e.g., Poage and Chamberlain, 2001; Rowley and Garzzone, 2007). Recent approaches to stable isotope-based paleoaltimetry include the application of compound-specific hydrogen isotope ratios of leaf-wax *n*-alkanes preserved in soils or sediments as a proxy to track the altitude effect on δD of precipitation (e.g., Polissar et al., 2009). Long chain *n*-alkanes are major lipid components of epicuticular leaf waxes produced by terrestrial higher plants (e.g., Eglinton and Hamilton, 1967). They are well-preserved in sediments and soils and their δD values have been shown to record changes in the δD values of meteoric water, modified by plant-specific effects and evapotranspiration (e.g., Sachse et al., 2012). Hence, an increasing number of studies have relied on *n*-alkane-based δD values for reconstructing the Neogene to present surface elevation history of high continental interiors such as the northern Sierra Nevada (Hren et al., 2010), the Tibetan Plateau (Polissar et al., 2009; Zhuang et al., 2014) and the Eastern Cordillera of Colombia (Anderson et al., 2015). Aside from soil *n*-alkane δD values, the distribution of branched glycerol dialkyl glycerol tetraethers (brGDGTs) in soils has also been documented to follow adiabatic cooling of air with increasing altitude (e.g., Sinninghe Damsté et al., 2008; Peterse et al., 2009). BrGDGTs are membrane lipids most likely derived from heterotrophic bacteria that vary in the number of methyl branches (four to six) and cyclopentane moieties (up to two) (e.g., Sinninghe Damsté et al., 2000). The number of methyl branches have been shown to depend primarily on mean annual air temperature (MAT) and to a lesser extent soil pH, while the number of cyclopentane moieties and the abundances of the six 6-methyl brGDGTs are predominantly related to soil pH (e.g., Weijers et al., 2007; De Jonge et al., 2014). BrGDGTs are ubiquitous and commonly well-preserved in soils, resulting in various applications related to the reconstruction of paleoelevation (e.g., Anderson et al., 2014, 2015; Coffinet et al., 2014; Zhuang et al., 2015). Predicted MAT values for alkaline soils from arid and semiarid regions, however, have consistently been underestimating actual MAT values (e.g., Peterse et al., 2012). Methodological advances, mainly the separation of a series of novel 6-methyl brGDGTs from their respective 5-methyl brGDGTs isomers (MAT_{mr} index = multiple linear regression-based MAT; De Jonge et al., 2014) resulted in reduced scatter in the soil calibration data and consequently more precise MAT and soil pH reconstructions for arid soils.

Given their latitudinal extent and elevation, the Andes constitute the most important orographic barrier to atmospheric circulation in the southern hemisphere. Today, the Andes intercept moisture-bearing winds on the eastern flanks in the north and on the western flanks in the south, thus providing a particularly suitable setting to study the interplay between surface elevation and stable isotopes in precipitation (e.g.,

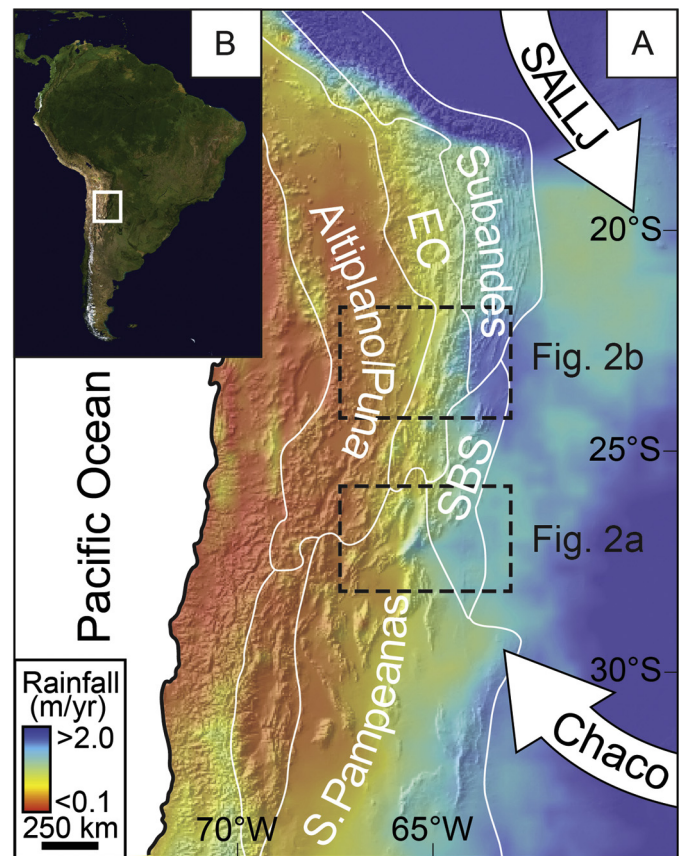


Fig. 1. A) Topographic map of the South Central Andes showing annual rainfall based on TRMM 3B42. Morphotectonic provinces: SBS = Santa Bárbara System, EC = Eastern Cordillera, S. Pampeanas = Sierras Pampeanas (modified from Rohrmann et al., 2014). Arrows highlight moisture transport (SALLJ = South American Low Level Jet) and orogenward-moisture transport controlled by the Chaco low. Black dashed boxes indicate the sampling transects in Fig. 2a (hillslope transect) and Fig. 2b (valley transect). White rectangle in B) shows location of the study area.

Confiantini et al., 2001; Rohrmann et al., 2014). The surface elevation history of the central Andes, however, is still widely debated. For at least the last 10–8 Myr, the Andes have blocked and deflected the northerly branch of trade winds from the equatorial Atlantic and Amazonia to form the South American Low-Level Jet (SALLJ) (e.g., Mulch et al., 2010). This barrier jet transports moisture southward along the eastern Andean flanks and turns clockwise around the Chaco Low, a continental thermal low-pressure system centered over northern Argentina (Fig. 1). At 200 hPa the Bolivian High anticyclone dominates over the Altiplano Plateau during the austral summer (December to February, DJF). The Bolivian High is induced by the surface sensible heat flux over the plateau and the latent heating rate of condensation released during precipitation (e.g., Lenters and Cook, 1997). Deep moisture convection during the austral summer is related to a vertically overturning circulation with a southward displacement and intensification of the Bolivian High and the reinforcement of the Chaco Low over the interior of the continent (e.g., Vuille, 1999). The seasonal distribution of precipitation in this region results in >80% of the annual rainfall during the austral summer (DJF) (e.g., Vera et al., 2006). The eastern Andean Cordillera today receives rainfall of 1000–3000 mm/yr and hence contrasts the dry intermontane basins with only 200 mm/yr or less (e.g., Bookhagen and Strecker, 2008). Focused precipitation along the eastern Andean flanks and leeward aridification are characteristic of the entire length of the South Central Andes. The precipitation gradients are reflected in the stable

isotope systematics of precipitation in the northern and central Andes. δD and $\delta^{18}O$ values of surface waters and precipitation across the Eastern Cordillera of Colombia (Saylor et al., 2009) and Bolivia (Gonfiantini et al., 2001) document that stable isotope-elevation relationships typically depict a linear relationship with decreasing δD and $\delta^{18}O$ values as a function of elevation. Similarly, TRMM satellite rainfall estimates and $\delta^{18}O$ values of water samples in the south central Andes reveal a clear relationship between rainfall and topographic relief due to orographic lifting and rain out (Bookhagen and Strecker, 2008; Rohrmann et al., 2014). However, between 22–28°S the impact of convective precipitation progressively increases southward resulting in a reduction of the river-based δD and $\delta^{18}O$ lapse rates along strike of the Andes (Rohrmann et al., 2014), documenting the necessity to understand the history of orographic versus convective rainfall in the region. Here we present a combined soil-derived δD *n*-alkane and temperature record from present-day elevation gradients in the central Andes from NW Argentina. In conjunction with soil temperature logger data we document systematic relationships between *n*-alkane δD values (δD_{C29}) and brGDGTs soil temperatures with elevation in two elevation gradients between 26–28°S and 22–24°S along the windward flanks of the Eastern Cordillera.

2. Material and methods

2.1. Sampling strategy

We devised a sampling strategy to track environmental and hydrological gradients along two altitudinal transects on the windward side of the South Central Andes that cover different topographic scenarios: a hillslope transect (26–28°S; $n = 8$) along the Río La Angostura that covers an elevation range of 290 to 3100 m directly up-slope and a valley transect (22–24°S; $n = 9$) along the Río Grande spanning a catchment elevation of 313 to 2458 m (Fig. 2a, b). In contrast to the hillslope transect, the Río Grande transect situated between two orographic uplifts transitions from the windward to the leeward side of the eastern Andean slopes and hence covers a large hydrological gradient. For comparison, we also included sites on the Altiplano–Puna plateau in the hillslope transect (AR11_S24 and AR11_S25 at 3574 and 3553 m, respectively; Fig. 2a) and a high elevation site in a tributary of the Río Grande valley transect (AR13_080 at 4130 m; Fig. 2b).

Soil samples were collected in March 2011 and March 2013. Soils were retrieved at 20 cm depth after removal of the litter and leaf layers and stored in paper bags. Elevation, latitude and longitude of each sampling location were recorded with portable GPS units. In the laboratory soil samples were air-dried, sieved through a 2 mm mesh size sieve and homogenized with an agate mortar. During the sampling campaigns a total of seven *in situ* soil temperature loggers (Votcraft DL-101T USB) were deployed along both transects at different elevations and buried at the same depth (20–25 cm) at which samples were taken. Soil temperature data were recorded hourly from March 2013 to March 2014 (Fig. 3a, b).

2.2. Extraction and fractionation of soil lipids

An aliquot of dried soil samples (15 g) was extracted with an accelerated solvent extractor (DIONEX 200) using a mixture of dichloromethane (DCM) and MeOH (9:1 v/v) at 100 °C and 7.6×10^6 Pa. The total lipid extract was separated into apolar and polar fractions using a Pasteur pipette column filled with activated Al_2O_3 and eluted with hexane and DCM/MeOH (1:1 v/v), respectively. Except for preparatory steps at the Biodiversity and Climate Research Centre (BiK-F) all analyses were performed at the NIOZ Royal Netherlands Institute for Sea Research.

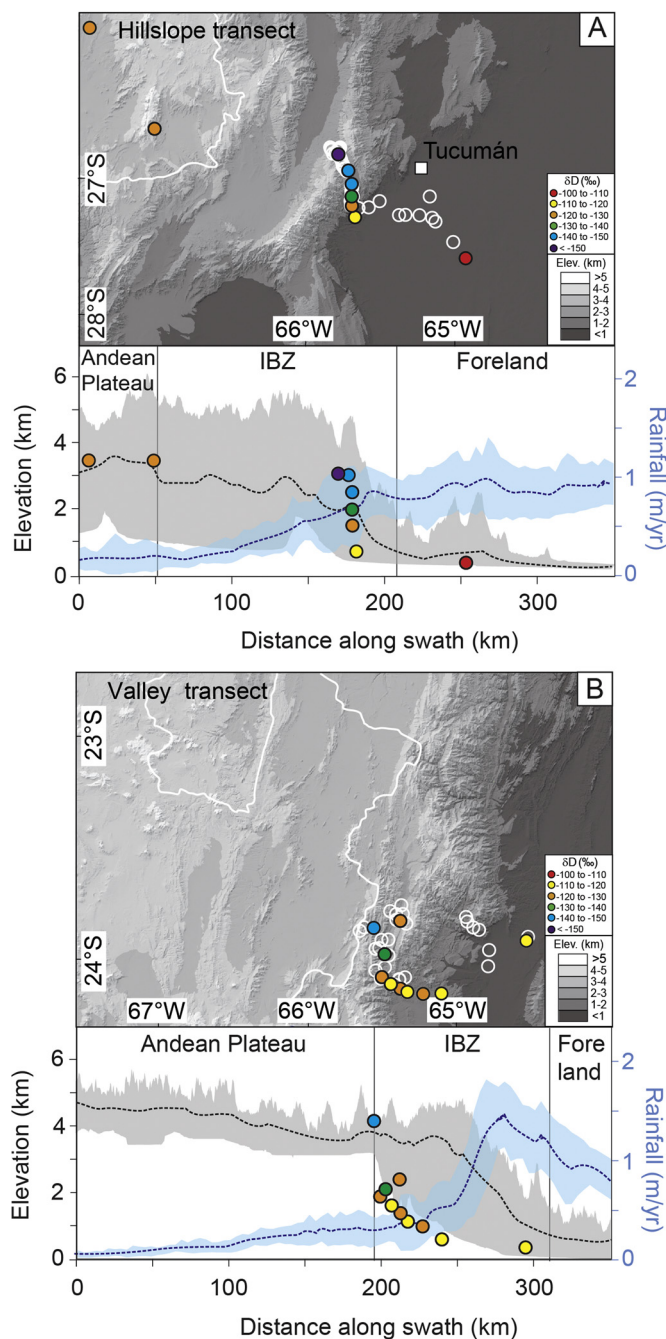


Fig. 2. Topographic map of the South Central Andes. Color-coded δD soil *n*-alkane values across two elevation transects: a hillslope transect along the Río La Angostura (A) and a valley transect along the Río Grande (B). Lower boxes show swath profiles including maximum, minimum (gray shading) and mean elevation (black dash line) and TRMM-2B31 rainfall data (blue). Stream-water sampling sites of Rohrmann et al. (2014) are indicated by white circles. The solid white line delineates the internally drained areas of the Puna Plateau. IBZ = Intermontane Basin Zone. (For interpretation of the references to color in this figure legend, the reader is referred to the web version of this article.)

2.3. Compound specific δD analysis of soil *n*-alkanes

The apolar fraction was re-dissolved in 30 μL of hexane. Analysis of *n*-alkanes was performed on a Hewlett Packard 6890 GC equipped with an on-column injector and flame ionization detector and a fused silica column (25 m \times 0.32 mm internal diameter) coated with CP Sil-5 (0.12 μm thickness) and He as mobile phase. The hydrogen isotopic composition of *n*-alkanes was determined

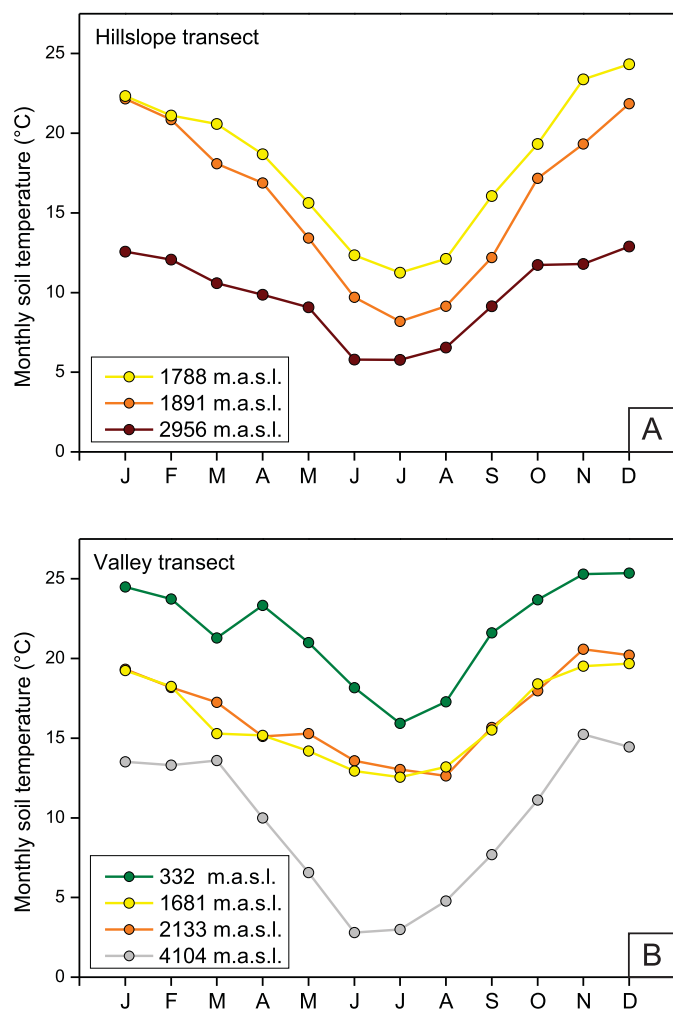


Fig. 3. *In situ* mean monthly soil temperatures recorded by temperature loggers along the hillslope (A) and valley (B) transects.

using a Thermo Electron DELTA Plus XL isotope ratio GC-MS. GC conditions were identical to those used in the analysis of *n*-alkanes except that the film thickness of the CP Sil-5 column was 0.4 μm with a constant He flow of 1.5 mL/min. Compounds were pyrolyzed at 1450 $^{\circ}\text{C}$ in an empty ceramic tube, which was pre-activated by a CH_4 flow of 0.5 mL/min for 5 min. H_2 gas of known isotopic composition was used as monitoring gas and a mixture of C_{16} – C_{32} *n*-alkanes, each of known isotopic composition (-42‰ to -256‰ vs. VSMOW) was used to monitor the performance of the system (Mix B, Schimmelmann, Indiana University). Samples were only analyzed if the average deviation of Mix B from the off-line determined values was 5 ‰ or less. Analyses were done in duplicate and squalane standards were co-injected with every sample.

2.4. Analysis of brGDGT

The polar fraction containing the GDGTs was dissolved in hexane/isopropanol (99:1 v/v) to a concentration of 2 mg/mL and filtered through a 0.45 μm PTFE filter attached to a 1 mL syringe. Analysis was performed using ultra high performance liquid chromatography-mass spectrometry (UHPLC-MS; Agilent 1260 coupled to an Agilent 6130 single quadrupole mass detector with an auto-injector) according to the procedure described by Hopmans et al. (2016). Detection was achieved using atmospheric pressure chemical ionization (APCI). Identification and quantification

of the different GDGT isomers were based on single ion monitoring (SIM, $[\text{M} + \text{H}]^+$ ions at m/z 1050, 1048, 1046, 1296, 1036, 1034, 1032, 1022, 1020 and 1018) and Chemstation software.

MAT_{mr} index was calculated based on linear combinations of the fractional abundances of the brGDGTs that correlate with MAT (De Jonge et al., 2014) where roman numerals in Eqs. (1) and (2) correspond to 5-methyl brGDGT with 4–6 methyl branches (I–III) containing 0–3 cyclopentane moieties (a–c).

$$\text{MAT}_{\text{mr}} = 7.17 + 17.1 \cdot [\text{Ia}] + 25.9 \cdot [\text{Ib}] + 34.4 \cdot [\text{Ic}] - 28.6 \cdot [\text{IIa}] \quad (1)$$

The BIT index (Branched versus Isoprenoid Tetraether index) was calculated according to Hopmans et al. (2004). Its value varies between 0 and 1, with high BIT values indicating GDGTs derived from terrestrial environments relative to crenarchaeol (especially abundant in marine and lacustrine environments), and vice versa. In Eq. (2) crenarchaeol contains four cyclopentane moieties and one cyclohexane moiety. The 6-methyl brGDGTs are indicated by a prime symbol after the roman numerals for their corresponding 5-methyl isomers:

$$\text{BIT} = \frac{([\text{IIIa}] + [\text{IIIa}'] + [\text{IIa}] + [\text{IIa}'] + [\text{Ia}])}{([\text{IIIa}] + [\text{IIIa}'] + [\text{IIa}] + [\text{IIa}'] + [\text{Ia}] + [\text{crenarchaeol}])} \quad (2)$$

3. Results

3.1. Soil *n*-alkane δD values

Identified soil *n*-alkanes exhibit a unimodal distribution between C_{27} and C_{33} with C_{29} being most abundant. Concentrations of *n*-alkanes extracted from the surface soils were high enough to accurately determine *n*-alkane δD in 19 of the 20 samples (Fig. 4, Table S1). Sample AR11_S05 was not analyzed for compound specific δD due to the low abundance of individual *n*-alkanes and presence of unsaturated hydrocarbon molecules, even after an additional purification/clean-up of the alkane fraction in hexane over an AgNO_3 impregnated silica-gel column. One sample (ST13_015) was excluded from further analysis due to the low abundance of compounds resulting in large standard errors (Table S1). The δD values of C_{29} *n*-alkanes along the hillslope transect ranged from -107‰ (290 m) to -164‰ (3100 m) with standard deviations between 0.5 ‰ and 6.9 ‰ (1σ), while the two uppermost samples within the Puna plateau showed δD values of -123‰ (3574 m) and -129‰ (3553 m) with standard deviations of 0.5 ‰ and 1.2 ‰ (1σ), respectively (Fig. 4a, Table S1). δD values from the valley transect ranged from -110‰ (313 m) to -145‰ (4130 m) with standard deviations between 1.2 ‰ and 5.4 ‰ (1σ) (Fig. 4b, Table S1). There is a high and significant correlation between the δD values of sedimentary leaf waxes and elevation at both transects ($R^2 = 0.91$, $p < 0.01$ at the hillslope transect and $R^2 = 0.76$, $p < 0.01$ at the valley transect) (Fig. 4a, b). Linear regression of the C_{29} *n*-alkane data provide δD lapse rates of $\Delta(\delta\text{D}) = -1.64\text{‰}/100\text{ m}$ at the hillslope transect (Fig. 4a) and $\Delta(\delta\text{D}) = -0.95\text{‰}/100\text{ m}$ at the valley transect (Fig. 4b).

3.2. Reconstructed brGDGTs temperatures and *in situ* soil temperatures

BrGDGT-reconstructed MAT_{mr} values along the hillslope transect range from 19.5 $^{\circ}\text{C}$ (340 m) to 2.9 $^{\circ}\text{C}$ (3100 m) (Fig. 5a), while the two uppermost samples within the Puna plateau show values of 3.2 $^{\circ}\text{C}$ (3574 m) and 2.7 $^{\circ}\text{C}$ (3553 m) (Table S2). BIT values for the soils from this transect vary between 0.9 and 1.0 except for one soil sample (AR11_S05, BIT = 0.8), while the two

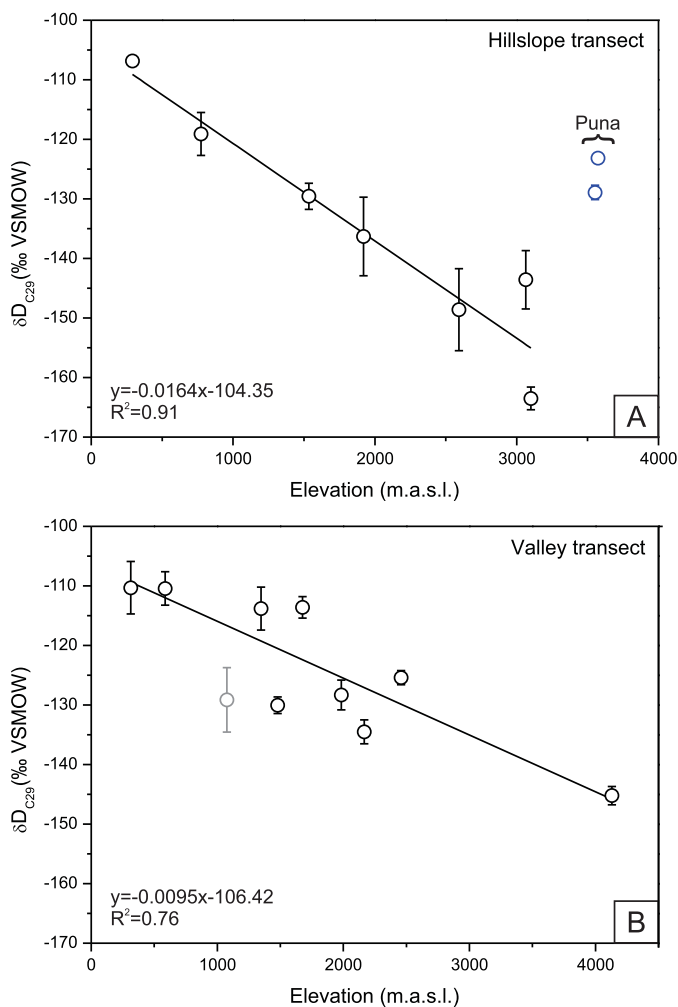


Fig. 4. δD values of soil n -alkane C_{29} across the hillslope (A) and valley (B) transects. Samples from the internally drained part of the Puna plateau indicated by blue circles. Sample in gray has been excluded from the linear interpolation due to the low abundance of compounds. (For interpretation of the references to color in this figure, the reader is referred to the web version of this article.)

uppermost samples within the Puna plateau show BIT values of 0.7 (3574 m) and 0.5 (3553 m) (Fig. 5a, Table S2). BrGDGT-reconstructed MATmr values along the valley transect range from 13.1 °C (313 m) to 7.3 °C (4130 m), while BIT values are generally low and vary between 0.4 and 0.9 (Fig. 5b, Table S2). Similar to the δD n -alkane values, brGDGT distributions correlate with altitude at both transects, reflecting the decrease of temperature with increasing elevation ($R^2 = 0.91$, $p < 0.01$ at the hillslope transect and $R^2 = 0.48$, $p < 0.05$ at the valley transect) (Fig. 5a, b). Linear regression of reconstructed MATmr values yields a temperature lapse rate of $\Delta T = -0.51$ °C/100 m at the hillslope transect (Fig. 5a) and $\Delta T = -0.19$ °C/100 m at the valley transect (Fig. 5b).

Mean monthly soil temperatures recorded by the temperature loggers show prominent soil temperature seasonality and a clear decrease in soil temperature with increasing elevation along the hillslope transect (Fig. 3a) and the valley transect (Fig. 3b). Measured soil temperatures vary between 11.9 °C (1788 m) and 6.0 °C (2956 m) during the winter (JJA) and 22.6 °C and 12.5 °C during the summer months (DJF) at the hillslope transect (Fig. 3a, Table S2). At the valley transect measured soil temperatures vary between 17.1 °C (332 m) and 13.1 °C (2133 m) during the winter (JJA) and 24.5 °C and 19.3 °C during the summer months (DJF)

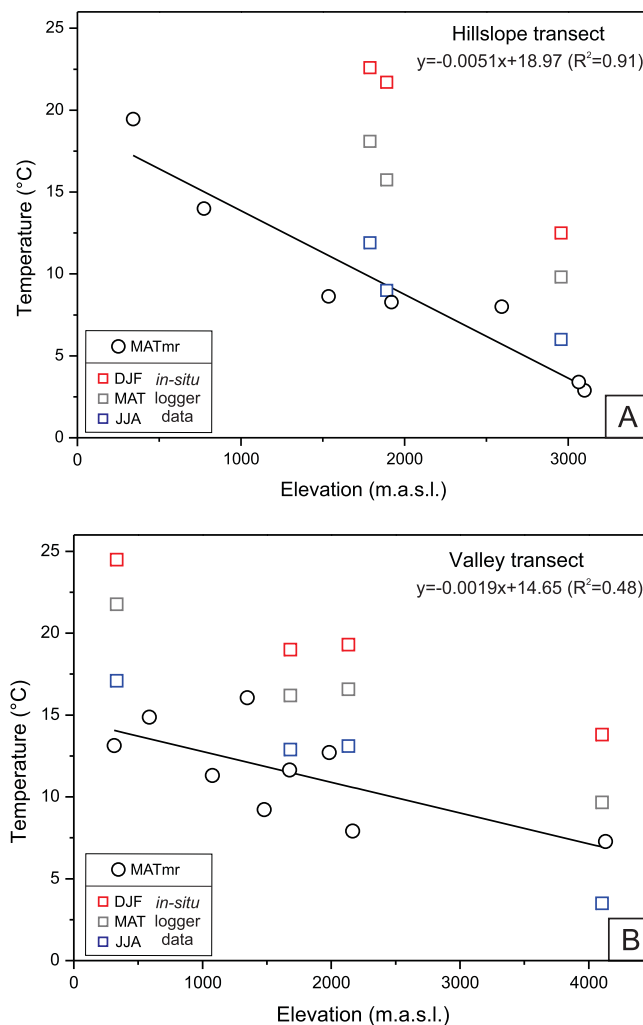


Fig. 5. Measured MAT from *in situ* soil temperature loggers (squares) and reconstructed MATmr based on the fractional abundance of all 15 soil brGDGTs as defined by De Jonge et al. (2014) (circles) along the hillslope (A) and valley (B) transects. MAT = mean annual temperature; MATmr = multiple linear regression-based MAT reconstruction; DJF = summer temperature; JJA = winter temperature.

(Fig. 3b, Table S2). Measured mean annual soil temperatures range between 18.1 °C and 9.8 °C at the hillslope transect (Fig. 5a, Table S2) and 21.8 °C and 16.6 °C at the valley transect (Fig. 5b, Table S2). Measured mean winter, summer and annual soil temperatures show a robust linear correlation with altitude along the hillslope with $\Delta T = -0.40$ °C/100 m, $R^2 = 0.82$, $p < 0.3$ for winter (JJA); $\Delta T = -0.90$ °C/100 m, $R^2 = 1.00$, $p < 0.01$ for summer (DJF) and $\Delta T = -0.65$ °C/100 m, $R^2 = 0.96$, $p < 0.05$ for annual soil temperatures (Fig. 5a). At the valley transect measured temperatures also show a robust linear correlation with altitude with $\Delta T = -0.40$ °C/100 m, $R^2 = 0.96$, $p < 0.05$ for winter (JJA); $\Delta T = -0.30$ °C/100 m, $R^2 = 0.97$, $p < 0.05$ for summer (DJF) and $\Delta T = -0.30$ °C/100 m, $R^2 = 0.98$, $p < 0.05$ for annual soil temperatures (Fig. 5b). The absolute values of reconstructed MATmr are consistently lower than measured mean annual soil temperatures in both transects (mean difference of 8.0 °C at the hillslope transect and 6.1 °C at the valley transect) (Fig. 6a, b, Table S2). Instead they approach absolute values, slopes and intercepts of measured average cold season (JJA) temperatures in both transects, with a mean difference of 2.4 °C at the hillslope transect and 3.6 °C at the valley transect (Fig. 5a, b, Table S2).

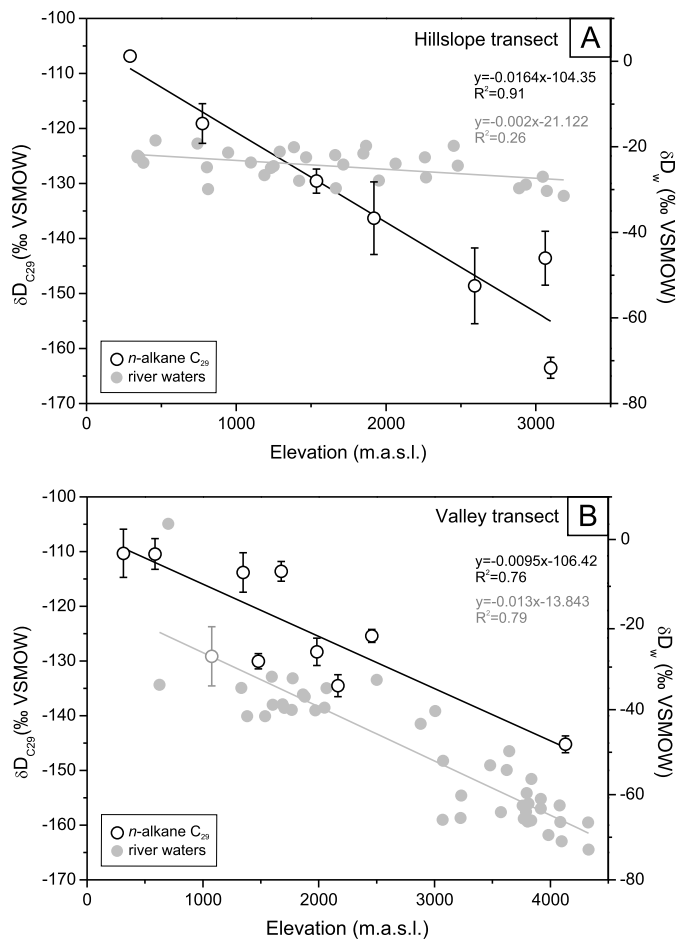


Fig. 6. δD values of soil n -alkane C_{29} and stream-water samples (gray circles) (Rohrmann et al., 2014) along the hillslope (A) and valley (B) transects. (For interpretation of the references to color in this figure legend, the reader is referred to the web version of this article.)

4. Discussion

4.1. Relationship between soil n -alkane δD values and elevation in the South Central Andes

Central Andean soil n -alkanes exhibit a strong odd-over-even carbon number predominance, indicating that they are mainly derived from epicuticular leaf waxes of terrestrial higher plants (Table S1) (Eglinton and Hamilton, 1967). δD n -alkane values decrease systematically with increasing elevation indicating that C_{29} n -alkane δD values record the effect of altitude on the δD of precipitation and soil water (Fig. 4a, b). Specifically, the isotope lapse rate in soil alkanes of the hillslope section ($\Delta(\delta D) = -1.64\text{‰}/100\text{ m}$, $R^2 = 0.91$, $p < 0.01$) falls within the range of hydrogen isotope elevation gradients from precipitation and surface waters in the Colombian Eastern Cordillera ($\Delta(\delta D) = -1.46\text{‰}/100\text{ m}$; Saylor et al., 2009), the equatorial Andes ($\Delta(\delta D) = -1.60\text{‰}/100\text{ m}$; Rozanski and Araguas-Araguas, 1995), the Peruvian Andes ($\Delta(\delta D) = -2.20\text{‰}/100\text{ m}$ in the wet season and $\Delta(\delta D) = -1.70\text{‰}/100\text{ m}$ in the dry season, Ponton et al., 2014) and the eastern Andean Cordillera in Bolivia ($\Delta(\delta D) = -1.30\text{‰}/100\text{ m}$, Bershaw et al., 2010; $\Delta(\delta D) = -1.90\text{‰}/100\text{ m}$ in rainy years and $\Delta(\delta D) = -1.20\text{‰}/100\text{ m}$ in dry years, Confiatini et al., 2001), yet differs from the river water lapse rate at the same latitude ($\Delta(\delta D) = -0.20\text{‰}/100\text{ m}$, Rohrmann et al., 2014, see discussion below). The apparent C_{29} n -alkane δD lapse rate is much lower along the valley transect ($\Delta(\delta D) = -0.95\text{‰}/100\text{ m}$,

$R^2 = 0.76$, $p < 0.01$ Fig. 4a) than along the hillslope transect ($\Delta(\delta D) = -1.64\text{‰}/100\text{ m}$, $R^2 = 0.91$, $p < 0.01$ Fig. 4b). This lower lapse rate along the valley transect is most likely due to the variable environmental conditions, most importantly the change from windward to leeward sampling position occurring along this altitudinal transect; i.e., the lower lapse rate is related to changes in hydrology along the valley sampling trajectory including changes in local vegetation. In contrast, the hillslope transect reflects the direct effects of orography on isotopes in precipitation, covering a forested environment with humid climate in the foreland-basin and semiarid to arid conditions at the highest elevations. Conversely, such a straightforward wet-to-dry transition is absent at the valley transect (Figs. 2, 4). The sampling trajectory along the valley, transitioning from the windward flank at low elevations to a leeward position at the uppermost sampling site, affects the apparent δD lapse rate. The uppermost soil sample located in the dry intermontane valley results in higher scatter of the δD versus altitude fit and hence a lower lapse rate (Figs. 2, 4). The similarity in the absolute δD values of the C_{29} n -alkane at elevations below ca. 2000 m for both transects points to altitude-dependent precipitation δD values being encoded in the C_{29} n -alkane δD data. With increasing elevation (and increasing leeward position with respect to the Tilcara Ranges to the W) C_{29} δD data along the valley transect are potentially biased to higher values similar to the elevated C_{29} δD data within the confines of the internally drained Puna plateau of the hillslope transect (see below). Overall, the valley transect data confirm that sedimentary leaf wax n -alkane δD values track shifts in precipitation δD values. This is also supported by the similar n -alkane δD lapse rate and linear correlation with altitude between the isotopic lapse rate obtained from leaf waxes at this valley transect in the Argentinean Andes ($\Delta(\delta D) = -0.95\text{‰}/100\text{ m}$, $R^2 = 0.76$, $p < 0.01$) and leaf wax n -alkane δD data from soil samples collected along a valley transect in the Peruvian Andes ($\Delta(\delta D) = -1.10\text{‰}/100\text{ m}$, $R^2 = 0.72$; Ponton et al., 2014).

The δD -elevation relationship directly obtained from the windward flanks of the hillslope transect breaks down in the internally drained part of the Puna plateau where δD values are D-enriched by up to $\sim 35\text{--}40\text{‰}$ when compared to soil samples located at the highest elevation of the hillslope transect (Fig. 4a, Table S1). The internally drained part of the Puna plateau contains abundant evaporite deposits as a result of sustained arid to hyper-arid conditions (less than 100 mm/yr rainfall) and vegetation typical for highly arid regions (halophytic grasses, shrubs) (e.g., Saylor et al., 2009). Although it is commonly assumed that δD values of sedimentary leaf wax n -alkanes record the isotopic composition of meteoric water, modified by plant-specific effects and evapotranspiration (e.g., Sachse et al., 2012), other factors such as vegetation composition, soil evaporation and plant transpiration likely enhance the deuterium content of soil and leaf water under such arid conditions (e.g., Feakins and Sessions, 2010). Consequently, the combined effects of both environmental conditions and vegetation in this region are the likely drivers for more positive δD n -alkanes values at the Puna plateau, thus affecting the relationship between plant wax δD values and altitude (Fig. 4a, Table S1). Changes in either aridity or vegetation composition have also been reported to cause enhanced D-enrichment of δD n -alkanes values that is independent of the isotopic composition of precipitation in soils from similar tropical environments in SE Mexico and N Central America (Douglas et al., 2012).

As sedimentary leaf waxes n -alkanes may record the hydrogen isotopic composition of meteoric water, we compare our soil n -alkane δD values with δD values of stream waters collected along the two same elevation transects (Rohrmann et al., 2014). The δD lapse rate and linear correlation with altitude of stream waters along the valley transect ($\Delta(\delta D) = -1.30\text{‰}/100\text{ m}$, $R^2 =$

0.79; $\Delta(\delta^{18}\text{O}) = -0.17\text{‰}/100\text{ m}$, $R^2 = 0.68$) (Rohrmann et al., 2014) is similar to that obtained from soil *n*-alkanes ($\Delta(\delta\text{D}) = -0.95\text{‰}/100\text{ m}$, $R^2 = 0.76$, $p < 0.01$) (Figs. 2, 6b). However, the river waters collected along the hillslope transect show a much shallower δD lapse rate ($\Delta(\delta\text{D}) = -0.20\text{‰}/100\text{ m}$, $R^2 = 0.26$; $\Delta(\delta^{18}\text{O}) = -0.02\text{‰}/100\text{ m}$, $R^2 = 0.17$) when compared to the soil *n*-alkanes ($\Delta(\delta\text{D}) = -1.64\text{‰}/100\text{ m}$, $R^2 = 0.91$, $p < 0.01$) (Figs. 2, 6a). The weak relationship between δD in river water and elevation has been interpreted to result from deep convection rather than simple orographic rain-out along this transect (Rohrmann et al., 2014). The apparent discrepancy between soil *n*-alkane and river water δD values along the hillslope transect may be attributed to the fact that water sampling occurred over the summer period, where more than 80% of the annual precipitation occurs (Rohrmann et al., 2014). Therefore, although convective precipitation is dominating the annual water budget *n*-alkane δD values may average over longer parts of the year because of the extended plant-growing season. Furthermore, a pronounced daily fog develops along this elevation gradient providing an additional plant water source similar to observations in other ecosystems such as the Atacama Desert (e.g., Evans and Ehleringer, 1994). Soil *n*-alkane δD values from leaf waxes integrate a diverse mixture of lipids over decades to centuries, whereas the isotopic signal from river waters is controlled by catchment hydrology and seasonality of convective storms that provide the bulk of the river water. It is therefore possible that *n*-alkane accumulation reflects an averaged temporal and spatial precipitation pattern in contrast to a more seasonal signature of the stream waters. Indeed, several studies have generally found much stronger correlation between catchment-integrated leaf-wax δD values from sedimentary archives and δD of precipitation in semi-arid to arid environments than with values recorded by individual plants (e.g., Feakins and Sessions, 2010). Given the arguments above we suggest that despite current convective rainfall dominance in the region *n*-alkane δD values from leaf waxes are robust recorders of averaged meteoric δD values, implying that the $\delta\text{D}_{\text{wax}}$ lapse-rate of $\Delta(\delta\text{D}) = -1.64\text{‰}/100\text{ m}$ ($R^2 = 0.91$, $p < 0.01$) along the hillslope transect may serve as a present-day validation value for paleoaltimetry studies in the South Central Andes and in other regions with similar hydrological conditions.

4.2. Application of brGDGT distributions along elevation transects in the South Central Andes

The BIT index is based on the relative abundance of non-isoprenoidal brGDGTs versus isoprenoid GDGT crenarchaeol, which is especially abundant in aquatic environments. In soils, BIT values usually range between 0.8 and 1 (e.g., Sinninghe Damsté et al., 2008). Soil samples at the valley transect exhibit generally lower BIT index values than soil samples at the hillslope transect (Table S2). Sample AR11_S04 (290 m) was collected at the lowest elevation within the valley transect. This sample resulted in a low BIT index (0.6) and MAT_{mr} value (6.5 °C at 290 m) (Table S2). The low BIT value suggests substantial aquatic production of crenarchaeol from the nearby Río Dulce, therefore this sample was excluded from further analysis. At the hillslope transect one sample (AR13_085, 2458 m) was collected from the surface of an alluvial fan. This sample likewise resulted in a low BIT index (0.4) and unrealistically low MAT_{mr} (−5.6 °C) (Table S2). Therefore this sample was also removed from further interpretation due to evidence of contribution of aquatic GDGTs.

Reconstructed MAT_{mr} values decrease systematically with increasing elevation and display a significant correlation with elevation along both altitudinal transects (Fig. 5). The MAT_{mr} lapse rate at the hillslope transect ($\Delta T = -0.51\text{ °C}/100\text{ m}$, $R^2 = 0.91$, $p < 0.01$) (Fig. 5a) is almost identical to the soil MAT lapse rate

obtained from *in situ* soil data loggers ($\Delta T = -0.65\text{ °C}/100\text{ m}$, $R^2 = 0.96$, $p < 0.01$) (Fig. 5a), as well as to the apparent lapse rate determined from MODIS land-surface temperatures at this transect ($\Delta T = -0.64\text{ °C}/100\text{ m}$, $R^2 = 0.74$) (Rohrmann et al., 2014) and the regional temperature lapse gradient acquired at ground level in weather stations along the Eastern Cordillera of Bolivia ($\Delta T = -0.50\text{ °C}/100\text{ m}$) (Gonfiantini et al., 2001). This lapse rate is also in the same range as previously found in soils from other regions of the world such as on Mount Rungwe and Kilimanjaro (Tanzania) ($\Delta T = -0.70\text{ °C}/100\text{ m}$; Sinninghe Damsté et al., 2008; Coffinet et al., 2014), Mount Gongga (China) ($\Delta T = -0.59\text{ °C}/100\text{ m}$; Peterse et al., 2009), the Southern Alps ($\Delta T = -0.56\text{ °C}/100\text{ m}$; Zhuang et al., 2015), the Eastern Cordillera of Colombia ($\Delta T = -0.49\text{ °C}/100\text{ m}$; Anderson et al., 2014) and on Mount Meghalaya (India) ($\Delta T = -0.48\text{ °C}/100\text{ m}$; Ernst et al., 2013). In contrast, the MAT_{mr} lapse rate along the valley transect ($\Delta T = -0.19\text{ °C}/100\text{ m}$, $R^2 = 0.48$, $p < 0.05$ Fig. 5b) differs from the hillslope transect ($\Delta T = -0.51\text{ °C}/100\text{ m}$, $R^2 = 0.91$, $p < 0.01$ Fig. 5a). This lower lapse rate along the valley transect is mainly controlled by the reconstructed temperature from the uppermost soil sample which yielded higher than expected temperatures at this altitude compared to MAT_{mr} values obtained at the hillslope transect (7.3 °C at 4130 m in the valley transect and 2.9 °C at 3100 m along the hillslope transect, Table S2). Higher radiative heating of the valley bottom at these altitudes combined with sparse vegetation cover might be responsible for the higher-than-expected soil temperature at this elevation and thus may have contributed to the apparent lower temperature lapse rate and the weaker temperature versus elevation fit. Nonetheless, the obtained lapse rate determined from the brGDGT-derived proxy at the valley transect ($\Delta T = -0.19\text{ °C}/100\text{ m}$, $R^2 = 0.48$, $p < 0.05$) resembles, to some extent, that from *in situ* soil data loggers ($\Delta T = -0.31\text{ °C}/100\text{ m}$, $R^2 = 0.98$, $p < 0.01$) (Fig. 5b).

Absolute brGDGT MAT values presented here are reconstructed according to the new MAT_{mr} index developed by De Jonge et al. (2014) (equation (1)), which relies on the relation of brGDGT distributions with mean annual air temperature. Comparison of these values and measured soil MAT obtained from *in situ* temperature loggers shows that absolute MAT_{mr} values are lower than measured soil MAT in both transects. At current we are unable to clearly distinguish whether the similarity to measured winter (JJA) soil temperatures implies that brGDGT distributions record winter soil temperature conditions (Fig. 5a, b) or whether the strong rainfall and temperature seasonality in these soils biases bacterial soil activity to particular soil water conditions. brGDGTs are ubiquitous in peatlands and soils, and their highest abundances have been found below the ground water table in the catotelm, the anoxic and permanently saturated layer of the peat bog (Weijers et al., 2009). Although their biological origin remains still unclear it is thought that they are mainly produced by bacteria (*Acidobacteria*) as supported by the identification of its potential “building block” (iso-diabolic acid) in some species of subdivisions 1, 3, and 4 *Acidobacteria* (e.g., Weijers et al., 2009; Sinninghe Damsté et al., 2014). In the South Central Andes, winter (JJA) is the cold and dry season and >80% of the annual rainfall takes place during the austral summer (DJF) (Vera et al., 2006). It is thus plausible that for this particular location and climate setting the brGDGT-producing organisms are preferably becoming more active after the summer tropical rainy season when soils are water saturated in winter and thus inducing favorable conditions for microbial activity. A series of studies have recently reported that brGDGT-derived temperature estimates are frequently biased towards the seasonal optimum for the growth of the brGDGT-producing bacteria (e.g., Peterse et al., 2012; Dirghangi et al., 2013; De Jonge et al., 2014; Menges et al., 2014). In particular, it has been noticed that MATs are typically underestimated in alkaline soils

from arid-subhumid climates most likely as a response to hydrological conditions such as soil water availability and precipitation amount, which serve as limiting factors controlling brGDGT distributions (e.g., Ernst et al., 2013; De Jonge et al., 2014; Wang et al., 2014). Such an underestimation may be due to the fact that the global soil calibration (De Jonge et al., 2014) to calculate MAT_{mr} does not fully account for local conditions (rainfall and temperature seasonality) at these elevations and latitude. Our data hence are in line with previous claims on soil water availability and precipitation amount as additional controls on brGDGTs distributions. Eventually, the reconstructed soil temperature lapse rates are consistent with *in situ* temperature lapse rates and regional observations and thus applicable for altitudinal studies along the south central Andes, at least when it comes to comparison of relative temperature change as a function of elevation. In addition the data presented here are consistent with quantitative temperature values derived from brGDGT distributions being biased after the rainy season in alkaline soils from arid-semiarid regions in the South Central Andes.

5. Implications for paleoaltimetry studies and conclusions

We have assessed the suitability of δD values of soil-derived *n*-alkane and brGDGT distributions along the eastern flanks of the southern central Andes as proxies for paleoaltimetry and paleoenvironmental reconstructions. Both proxies show a significant linear correlation with altitude, thus proving to be applicable for estimating paleoelevation across steep orographic gradients in the south central Andes and in regions with similar hydrological conditions. Present-day isotopic and brGDGT-derived temperature lapse rates at the hillslope transect ($\Delta(\delta D) = -1.64\text{‰}/100\text{ m}$, $R^2 = 0.91$, $p < 0.01$ and $\Delta T = -0.51\text{ °C}/100\text{ m}$, $R^2 = 0.91$, $p < 0.01$) broadly follow the slopes from other tropical regions in the Andes and from *in situ* soil temperature measurements and we consider the hillslope transect to best reflect the impact of orography on δD values in precipitation. δD values from leaf waxes most likely reflect a temporally integrated signal over time scales of hundreds of years, thus being less sensitive to changes in seasonality than approaches based on river waters or short-term station sampling campaigns ($\Delta(\delta D) = -0.20\text{‰}/100\text{ m}$, $R^2 = 0.26$). However, hydrological and environmental effects seem to have a significant influence on the spatial variability of *n*-alkane δD values when increasing arid conditions and changes in vegetation composition at the Puna Plateau are reflected by much more D-enriched values.

In the geographically (and climatically) more complex valley transect hydrogen isotope lapse rates are lower with significantly higher scatter ($\Delta(\delta D) = -0.95\text{‰}/100\text{ m}$, $R^2 = 0.76$, $p < 0.01$ and $\Delta T = -0.19\text{ °C}/100\text{ m}$, $R^2 = 0.48$, $p < 0.05$) due to the windward-leeward transition sampled across this elevation transect. Additional sampling between 2500 m and 4130 m might improve the lapse rates obtained at this transect, but soil samples recovered at 2458 m from the surface of an alluvial fan showed evidence of aquatic GDGTs (BIT index = 4), resulting in unrealistically low MAT_{mr} values (MAT_{mr} = -5.6 °C).

Absolute values of brGDGT-derived MAT_{mr} are biased towards the cold and dry austral winter season, when soils are water saturated after the summer rainy season, suggesting that the distribution of brGDGTs is influenced by precipitation amount and/or water saturation. It is also plausible that the use of a global calibration for the reconstruction of MAT in this region has resulted in systematically colder temperatures. If so, local calibrations would become beneficial for these particular arid and alkaline conditions in order to improve the accuracy of brGDGT-derived temperature estimates. Hence, our data document that δD *n*-alkane and brGDGTs distributions can be used over time scales relevant for paleoclimate/altimetry reconstructions but also stress that such

reconstructions require previous knowledge of the depositional environment. Therefore, hydrological conditions, patterns of atmospheric circulation and their influence on δD values and brGDGT distributions need to be considered in arid environments and alkaline soils in order to reconstruct elevation histories.

Acknowledgments and funding

This study was funded by the Deutsche Forschungsgemeinschaft (DFG grants: STR 373/32-1 and MU2845/4-1) with support from the DFG-Leibniz Center for Surface Processes and Climate Studies at Universität Potsdam, the LOEWE funding program of Hesse's Ministry of Higher Education, Research, and the Arts, and the European Research Council under the Seventh Framework Programme (COFUND, Goethe University International Postdoc Programme GO-IN, No. 291776). MvdM was funded by the Dutch Organisation for Scientific Research (NWO) through a VIDI grant (N° 864.09.011). JSSD is supported by the Netherlands Earth System Science Center (NESSC). We are grateful to J. Ossebaard (NIOZ), D. Sinke-Schoen (NIOZ) and U. Treffert (BiK-F) for laboratory assistance and helpful discussions.

Appendix A. Supplementary material

Supplementary material related to this article can be found online at <http://dx.doi.org/10.1016/j.epsl.2016.07.049>.

References

- Anderson, V.J., Shanahan, T.M., Saylor, J.E., Horton, B.K., Mora, A.R., 2014. Sources of local and regional variability in the MBT'/CBT paleotemperature proxy: insights from a modern elevation transect across the Eastern Cordillera of Colombia. *Org. Geochem.* 69, 42–51.
- Anderson, V.J., Saylor, J.E., Shanahan, T.M., Horton, B.K., 2015. Paleoelevation records from lipid biomarkers: application to the tropical Andes. *Geol. Soc. Am. Bull.* 127 (11–12), 1604–1616.
- Bershaw, J., Garzione, C.N., Higgins, P., MacFadden, B.J., Anaya, F., Alvarenga, H., 2010. Spatial-temporal changes in Andean plateau climate and elevation from stable isotopes of mammal teeth. *Earth Planet. Sci. Lett.* 289, 530–538.
- Bookhagen, B., Strecker, M.R., 2008. Orographic barriers, high-resolution TRMM rainfall, and relief variations along the eastern Andes. *Geophys. Res. Lett.* 35, L06403.
- Chamberlain, C.P., Poage, M.A., Craw, D., Reynolds, R.C., 1999. Topographic development of the Southern Alps recorded by the isotopic composition of authigenic clay minerals, South Island, New Zealand. *Chem. Geol.* 155, 279–294.
- Coffinet, S., Huguet, A., Williamson, D., Fosse, C., Derenne, S., 2014. Potential of GDGTs as a temperature proxy along an altitudinal transect at Mount Rungwe (Tanzania). *Org. Geochem.* 68, 82–89.
- De Jonge, C., Hopmans, E.C., Zell, C.I., Kim, J.H., Schouten, S., Sinninghe Damsté, J.S., 2014. Occurrence and abundance of 6-methyl branched glycerol dialkyl glycerol tetraethers in soils: implications for palaeoclimate reconstruction. *Geochim. Cosmochim. Acta* 141, 97–112.
- Dirghangi, S.S., Pagani, M., Hren, M.T., Tipple, B.J., 2013. Distribution of glycerol dialkyl glycerol tetraethers in soils from two environmental transects in the USA. *Org. Geochem.* 59, 49–60.
- Douglas, P.M.J., Pagani, M., Brenner, M., Hodell, D.A., Curtis, J.H., 2012. Aridity and vegetation composition are important determinants of leaf-wax δD values in southeastern Mexico and Central America. *Geochim. Cosmochim. Acta* 97, 24–45.
- Eglinton, G., Hamilton, R.J., 1967. Leaf epicuticular waxes. *Science* 156, 1322–1335.
- Ehlers, T.A., Poulsen, C.J., 2009. Influence of Andean uplift on climate and paleoaltimetry estimates. *Earth Planet. Sci. Lett.* 281, 238–248.
- Ernst, N., Peterse, F., Breitenbach, S.F.M., Syiemlieh, H.J., Eglinton, T.I., 2013. Biomarkers record environmental changes along an altitudinal transect in the wettest place on Earth. *Org. Geochem.* 60, 93–99.
- Evans, R.D., Ehleringer, J.R., 1994. Plant $\delta^{15}\text{N}$ values along a fog gradient in the Atacama Desert, Chile. *J. Arid Environ.* 28, 189–193.
- Feakins, S.J., Sessions, A.L., 2010. Controls on the D/H ratios of plant leaf waxes in an arid ecosystem. *Geochim. Cosmochim. Acta* 74, 2128–2141.
- Garzione, C.N., Hoke, G.D., Libarkin, J.C., Withers, S., MacFadden, B., Eiler, J., Ghosh, P., Mulch, A., 2008. Rise of the Andes. *Science* 320, 1304–1307.
- Garzione, C.N., Quade, J., DeCelles, P.G., English, N.B., 2000. Predicting paleoelevation of Tibet and the Himalaya from $\delta^{18}\text{O}$ vs. altitude gradients in meteoric water across the Nepal Himalaya. *Earth Planet. Sci. Lett.* 183, 215–229.
- Gébelin, A., Mulch, A., Teyssier, C., Jessup, M.J., Law, R.D., Brunel, M., 2013. The Miocene elevation of Mount Everest. *Geology* 41 (7), 799–802.

- Gonfiantini, R., Roche, M.A., Olivry, J.C., Fontes, J.C., Zuppi, G.M., 2001. The altitude effect on the isotopic composition of tropical rains. *Chem. Geol.* 181, 147–167.
- Hoorn, C., Mosbrugger, V., Mulch, A., Antonelli, A., 2013. Biodiversity from mountain building. *Nat. Geosci.* 6, 154.
- Hopmans, E.C., Weijers, J.W.H., Schefuß, E., Herfort, L., Sinninghe Damsté, J.S., Schouten, S., 2004. A novel proxy for terrestrial organic matter in sediments based on branched and isoprenoid tetraether lipids. *Earth Planet. Sci. Lett.* 224, 107–116.
- Hopmans, E.C., Schouten, S., Sinninghe Damsté, J.S., 2016. The effect of improved chromatography on GDGT-based palaeoproxies. *Org. Geochem.* 93, 1–6.
- Hren, M.T., Pagani, M., Erwin, D.M., Brandon, M., 2010. Biomarker reconstruction of the early Eocene paleotopography and paleoclimate of the northern Sierra Nevada. *Geology* 38, 7–10.
- Lenters, J.D., Cook, K.H., 1997. On the origin of the Bolivian high and related circulation features of the South American climate. *J. Atmos. Sci.* 54, 656–678.
- Menges, J., Huguet, C., Alcañiz, J.M., Fietz, S., Sachse, D., Rosell-Melé, A., 2014. Influence of water availability in the distributions of branched glycerol dialkyl glycerol tetraether in soils of the Iberian Peninsula. *Biogeosciences* 11, 2571–2581.
- Mulch, A., 2016. Stable isotope paleoaltimetry and the evolution of landscapes and life. *Earth Planet. Sci. Lett.* 433, 180–191.
- Mulch, A., Sarna-Wojcicki, A.M., Perkins, M.E., Chamberlain, C.P., 2008. A Miocene to Pleistocene climate and elevation record of the Sierra Nevada (California). *Proc. Natl Acad. Sci.* 105, 6819–6824.
- Mulch, A., Uba, C.E., Strecker, M.R., Schoenberg, R., Chamberlain, C.P., 2010. Late Miocene climate variability and surface elevation in the central Andes. *Earth Planet. Sci. Lett.* 290, 173–182.
- Peterse, F., van der Meer, M.T.J., Schouten, S., Jia, G., Ossebaar, J., Blokker, J., Sinninghe Damsté, J.S., 2009. Assessment of soil *n*-alkane δD and branched tetraether membrane lipid distributions as tools for paleoelevation reconstruction. *Biogeosciences* 6, 2799–2807.
- Peterse, F., van der Meer, J., Schouten, S., Weijers, J.W.H., Fierer, N., Jackson, R.B., Kim, J.H., Sinninghe Damsté, J.S., 2012. Revised calibration of the MBT-CBT paleotemperature proxy based on branched tetraether membrane lipids in surface soils. *Geochim. Cosmochim. Acta* 96, 215–229.
- Poage, M.A., Chamberlain, C.P., 2001. Empirical relationships between elevation and the stable isotope composition of precipitation and surface waters: considerations for studies of paleoelevation change. *Am. J. Sci.* 301, 1–15.
- Polissar, P.J., Freeman, K.H., Rowley, D.B., McInerney, F.A., Currie, B.S., 2009. Paleoaltimetry of the Tibetan Plateau from D/H ratios of lipid biomarkers. *Earth Planet. Sci. Lett.* 287, 64–76.
- Ponton, C., West, A.J., Feakins, S.J., Galy, V., 2014. Leaf wax biomarkers in transit record river catchment composition. *Geophys. Res. Lett.* 41, 6420–6427.
- Poulsen, C.J., Ehlers, T.A., Insel, N., 2010. Onset of convective rainfall during gradual Late Miocene rise of the Central Andes. *Science* 328, 490–493.
- Rohrmann, A., Strecker, M.R., Bookhagen, B., Mulch, A., Sachse, D., Pingel, H., Alonso, R.N., Schildgen, T.F., Montero, C., 2014. Can stable isotopes ride out the storms? The role of convection for water isotopes in models, records, and paleoaltimetry studies in the central Andes. *Earth Planet. Sci. Lett.* 407, 187–195.
- Rowley, D.B., Garzione, C.N., 2007. Stable isotope-based paleoaltimetry. *Annu. Rev. Earth Planet. Sci.* 35, 463–508.
- Rowley, D.B., Pierrehumbert, R.T., Currie, B.S., 2001. A new approach to stable isotope-based paleoaltimetry: implications for paleoaltimetry and paleohypsometry of the High Himalaya since the Late Miocene. *Earth Planet. Sci. Lett.* 188, 253–268.
- Rozanski, K., Araguas-Araguas, L., 1995. Spatial and temporal variability of stable isotope composition of precipitation over the South American Continent. *Bull. Inst. Fr. Étud. Andin.* 24, 379–390.
- Sachse, D., Billault, I., Bowen, G.J., Chikaraishi, Y., Dawson, T.E., Feakins, S.J., Freeman, K.H., Magill, C.R., McInerney, F.A., van der Meer, M.T.J., Polissar, P., Robins, R.J., Sachs, J.P., Schmidt, H.L., Sessions, A.L., White, J.W.C., West, J.B., Kahmen, A., 2012. Molecular paleohydrology: interpreting the hydrogen-isotopic composition of lipid biomarkers from photosynthesizing organisms. *Annu. Rev. Earth Planet. Sci.* 40, 221–249.
- Saylor, J.E., Mora, A., Horton, B.K., Nie, J., 2009. Controls on the isotopic composition of surface water and precipitation in the Northern Andes, Colombian Eastern Cordillera. *Geochim. Cosmochim. Acta* 73, 6999–7018.
- Sinninghe Damsté, J.S., Hopmans, E.C., Pancost, R.D., Schouten, S., Geenevasen, J.A.J., 2000. Newly discovered non-isoprenoid glycerol dialkyl glycerol tetraether lipids in sediments. *Chem. Commun.*, 1683–1684.
- Sinninghe Damsté, J.S., Ossebaar, J., Schouten, S., Verschuren, D., 2008. Altitudinal shifts in the branched tetraether lipid distribution in soil from Mt. Kilimanjaro (Tanzania): implications for the MBT/CBT continental palaeothermometer. *Org. Geochem.* 39, 1072–1076.
- Sinninghe Damsté, J.S., Rijpstra, W.I.C., Hopmans, E.C., Foesel, B.U., Wüst, P.K., Overmann, J., Tank, M., Bryant, D.A., Dunfield, P.F., Houghton, K., Stott, M.B., 2014. Ether- and ester-bound iso-diabolic acid and other lipids in members of Acidobacteria Subdivision 4. *Appl. Environ. Microbiol.* 80, 5207–5218.
- Vera, C., Higgins, W., Amador, J., Ambrizzi, T., Garreaud, R., Gochis, D., Gutzler, D., Lettenmaier, D., Marengo, J., Mechoso, C.R., Nogues-Paegle, J., Dias, P.L.S., Zhang, C., 2006. Toward a unified view of the American Monsoon Systems. *J. Climate* 19, 4977–5000.
- Vuille, M., 1999. Atmospheric circulation over the Bolivian Altiplano during dry and wet periods and extreme phases of the Southern Oscillation. *Int. J. Climatol.* 19, 1579–1600.
- Wang, H., Liu, W., Zhang, C.L., 2014. Dependence of the cyclization of branched tetraethers on soil moisture in alkaline soils from arid-subhumid China: implications for palaeorainfall reconstructions on the Chinese Loess Plateau. *Biogeosciences* 11, 6755–6768.
- Weijers, J.W.H., Schouten, S., van den Donker, J.C., Hopmans, E.C., Sinninghe Damsté, J.S., 2007. Environmental controls on bacterial tetraether membrane lipid distribution in soils. *Geochim. Cosmochim. Acta* 71, 703–713.
- Weijers, J.W.H., Panoto, E., van Bleijswijk, J., Schouten, S., Rijpstra, W.I.C., Balk, M., Stams, A.J.M., Sinninghe Damsté, J.S., 2009. Constraints on the biological sources of the orphan branched tetraether membrane lipids. *Geomicrobiol. J.* 26, 402–414.
- Zhuang, G., Brandon, M.T., Pagani, M., Krishnan, S., 2014. Leaf wax stable isotopes from Northern Tibetan Plateau: implications for uplift and climate since 15 Ma. *Earth Planet. Sci. Lett.* 390, 186–198.
- Zhuang, G., Pagani, M., Chamberlain, C., Strong, D., Vandergoes, M., 2015. Altitudinal shift in stable hydrogen isotopes and microbial tetraether distribution in soils from the Southern Alps, NZ: implications for paleoclimatology and paleoaltimetry. *Org. Geochem.* 79, 56–64.